JOURNAL OF SPACECRAFT AND ROCKETS
Vol. 42, No. 6, November–December 2005

Sub-Boundary-Layer Disturbance Effects on Supersonic Base-Pressure Fluctuations

Jonathan R. Janssen*
ATK-Thiokol Propulsion, Promontory, Utah 84307
and
J. Craig Dutton†
University of Texas at Arlington, Arlington,Texas 76019

Fluctuating base pressures were measured for an axisymmetric blunt afterbody modified with two different sub-boundary-layer disturbance tabs, a triangle-tab configuration, and a strip-tab configuration, in a Mach 2.46 flowfield. Normalized rms levels indicate that base-pressure fluctuations increase with addition of the triangle tabs and decrease with the addition of the strip tab. Power-spectral-density (PSD) estimates recorded at the two outermost radial locations for the triangle-tab configuration demonstrated that the fluctuation energy increased when compared to the no-tab case at nearly all frequencies, particularly at frequencies above 1 kHz. This suggests that the triangular tabs energize turbulent structures in the free shear layer because of the introduction of streamwise vorticity. It was also found that a prominent peak in the PSD estimate at the outer two radial locations, found in the no-tab case, is absent for the triangle-tab configuration. Dual-transducer measurements for both tab configurations suggest that correlated pressure fluctuations are realized at most locations across the base simultaneously, lending credence to the idea that a global mechanism acts as a source of the base-pressure fluctuations.

Nomenclature

f_k	=	discrete frequency
G_{pp}, G_{xx}, or G_{yy}	=	one-sided power spectral density function for a general time-series history
G_{xy}	=	one-sided cross power spectral density function for two general time-series histories
h	=	height of the disturbance
i	=	given time
M	=	Mach number
N_t	=	total number of samples in the time series record
P_b	=	static pressure on the base surface
$\overline{P_b}$	=	area-averaged base pressure
P_{fs}	=	static pressure of the freestream fluid
P_{rms}	=	rms pressure
R_0	=	afterbody base radius
r	=	radial location on the base
x_i	=	individual time-series value
$\bar{x}$	=	average of time-series record
$\hat{x}$	=	rms of time-series record
γ_{xy}^2	=	coherence function for two general time-series histories
δ_0	=	boundary-layer thickness at separation
θ	=	afterbody base circumferential location

Introduction

SEPARATED supersonic flowfields, such as those near the bases of missiles and projectiles, are subjected to strongly favorable pressure gradients occurring at the base corner because of the expansion fan and separation of the boundary layer. Upon separation, a free shear layer that controls mixing between the high-speed inviscid freestream fluid and the low-speed base recirculation flow is formed.[1,2] The amount of mixing in the free shear laye controls mass entrainment from the recirculation region, which, in turn, sets base pressure. Previous measurements on an Army 155-mm M549 projectile by Rollstin[3] have shown that base drag, caused by the low pressure in the recirculation region, accounts for as much as 35% of the total drag. Because base drag is responsible for such a large percentage of the total drag, engineers and scientists have been developing methods to alter base pressure and total drag for many years. Among several methods commonly used to increase base pressure, and hence reduce total drag, are boattailing of the projectile and mass injection (bleed) into the recirculation region.

More recently, researchers have begun to investigate altering turbulent structures in the free shear layer to control mixing between the fluid entrained from the base recirculation region and that from the freestream. Alteration of the turbulent structures is typically achieved through disturbances to the boundary layer just upstream of separation. A relatively simple method of altering the boundary layer is through the use of boundary-layer disturbance tabs. In general, these tabs are designed to alter the boundary layer at or near separation. Alterations to the boundary layer typically take the form of modified turbulent structures or vortices, which then form an altered free shear layer upon separation. Tabs of various shapes, heights, configurations, and surface roughness have previously been examined for both planar and axisymmetric shear layers, jets, and base flows.[4–11] Initial studies concluded that tabs with heights on the order of the boundary-layer thickness only slightly altered the downstream free shear-layer characteristics.[4–6] These studies recorded minimal growth rate increases that were primarily attributed to increased boundary-layer thickness before separation. However, more recent studies using tabs with heights less than the boundary-layer thickness have recorded notable differences in free shear-layer characteristics, such as growth rate, without significantly increasing the boundary-layer thickness before separation.

Early measurements demonstrating increased entrainment and mixing in a compressible axisymmetric free shear layer were reported by King et al.[7] and Krothapalli et al.[8] Placing triangular and rectangular tabs of heights less than the boundary-layer thickness near the exit of an axisymmetric nozzle, these authors examined the effects of various tab dimensions and configurations on the downstream shear layer. Schlieren and laser-sheet flow visualizations

Received 11 August 2004; revision received 23 December 2004; accepted for publication 26 January 2005.

*Technical Staff, Ballistics and Grain Design Division. Member AIAA.
†Professor and Chair, Mechanical and Aerospace Engineering Department. Associate Fellow AIAA.

demonstrated that triangular tabs provided a mechanism to generate significant streamwise vorticity and, thereby, increased entrainment and mixing in the shear layer. Results from this study suggested that six triangular tabs with an apex angle of 25–30 deg, a height of 6 mm, and a thickness of 0.06 mm ($h/\delta_0 \approx 0.10$) equally spaced circumferentially around the nozzle was the most effective configuration to increase mixing. Further, they concluded that streamwise vortices could only be established if the natural amplification process were accelerated by a finite amplitude three-dimensional input.

A more extensive investigation of different tab geometries, configurations, and surface roughness was conducted on a compressible two-dimensional shear layer by Island et al.[9] These authors used planar laser-induced fluorescence and planar Rayleigh/Mie scattering (PRMS) to examine the effects of tabs on shear-layer growth and mass entrainment. Again, this study demonstrated that triangular tabs (three-dimensional disturbances), placed on the supersonic side of the splitter plate, is the configuration most effective at increasing shear-layer growth and mixing. They found that the optimum sub-boundary-layer disturbance increased shear-layer growth rate by 45% and the absolute shear-layer thickness by 48%. On the other hand, rectangular shapes (two-dimensional disturbances) were the least effective at increasing shear-layer thickness and growth rates. These results suggested that increased molecular mixing is primarily accomplished by thickening of the shear layer (i.e., increased mass entrainment). They concluded that three-dimensional disturbances induce streamwise structures, most likely counter-rotating pairs of vortices that are responsible for increased growth and thickening.

Bourdon and Dutton[10,11] and Bourdon[12] investigated the effects of tabs on a supersonic axisymmetric base flow. They studied a variety of triangular-tab[10] and strip-tab[11] (rectangular) configurations using mean base-pressure measurements and PRMS flow visualizations. Time-averaged pressure measurements on the base demonstrated that the triangular-tab configurations decreased the mean base pressure by as much as 10%. On the other hand, the optimum strip-tab configuration increased base pressure by slightly more than 3%. Using the results from the mean base-pressure measurements, Bourdon and Dutton selected two geometries to investigate the mechanisms responsible for altering base pressure with flow visualizations.[12] PRMS imaging showed that shear-layer growth near the base is significantly increased for the triangular-tab configuration as compared to the no-tab case. This was primarily attributed to an increase in streamwise vorticity generated by the tabs. The increased growth rate was responsible for increased mixing and higher mass entrainment from the recirculation region, resulting in lower base pressure (i.e., increased base drag). Visualizations for the strip-tab configuration showed that growth rates near the base were reduced compared to those for the no-tab base, indicating reduced mixing and mass entrainment from the recirculation region, which are responsible for the increased base pressure (i.e., reduced base drag). Instantaneous PRMS images provide direct evidence demonstrating differences between the shear-layer behavior for the triangle-tab, strip-tab, and no-tab cases. However, the physical mechanisms behind these differences are still not well understood or quantified. Further quantitative measurements for these cases can provide direct evidence to aid in determining the mechanisms responsible for altering the shear layer of these tabbed geometries.

Because base pressure is essentially set by the amount of mass entrained from the recirculation region by the shear layer, detailed, time-series base-pressure measurements can provide evidence as to the physical mechanisms responsible for altering the shear layer and, hence, base pressure. By altering various physical mechanisms in the shear layer through the use of tabs, the amount of fluctuation energy at various frequencies will be affected, and the results can be quantitatively recorded through the use of high-frequency pressure measurements in the base region. Thus, the mechanisms that control base pressure can begin to be quantified. The current study reports base-pressure fluctuation measurements for an axisymmetric afterbody in supersonic flow with both triangle and strip-tab disturbances mounted on the afterbody near the base corner. These measurements are compared extensively to similar measurements reported previously for the no-tab case.[13]

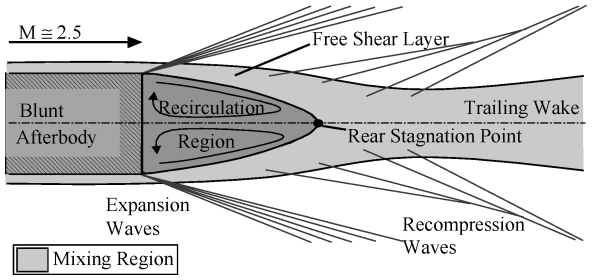

Fig. 1 Schematic of the time-averaged supersonic flow over an axisymmetric blunt afterbody.

Experimental Facilities and Procedures

Measurements of supersonic axisymmetric base-pressure fluctuations were completed in an axisymmetric wind tunnel located in the University of Illinois Gas Dynamics Laboratory. The axisymmetric wind tunnel consists of a stagnation chamber, a flow-conditioning unit, an annular converging-diverging nozzle, a sting-supported afterbody, a test section, and a diffuser.

Because the sting is supported far upstream of the flow-conditioning unit, measurements in the test section are relatively interference free. Attached to the end of the sting, the cylindrical blunt afterbody contains both radially and circumferentially located ports used for mounting high-frequency response pressure transducers. The afterbody has a nominal base diameter of 63.5 mm. A schematic of the time-averaged flowfield for this blunt-base geometry is shown in Fig. 1. During operation, the wind tunnel is run at a stagnation pressure of 499.2 ± 2.1 kPa and a stagnation temperature of 294.5 ± 0.3 K. In the wind-tunnel test section, the freestream Mach number before separation at the base corner is approximately 2.46 with a unit Reynolds number of 52×10^6 m^{-1}, whereas turbulence levels in the freestream are typically on the order of 1%. The incoming boundary-layer thickness just before separation at the base corner is 3.2 mm (Ref. 1). For further details on the test section and afterbody design, refer to Janssen and Dutton[13] and Herrin and Dutton.[1]

Mounted on the blunt axisymmetric afterbody near separation were sub-boundary-layer disturbance tabs. Two different tab configurations were used in the current investigation. These configurations were chosen based on time-averaged base-pressure measurements from a previous sub-boundary-layer disturbance investigation on a virtually identical axisymmetric afterbody.[11,12] Tabs were constructed by layering label sheets to achieve the desired thickness and then cutting out the desired shape. The first tab configuration examined utilized eight isosceles triangular tabs with the following dimensions: a thickness of 0.5 mm ($h/\delta_0 \approx 0.16$), a triangle height of 12.5 mm, and an apex angle of 30 deg. One of the triangular tabs was aligned with the radially mounted transducers on the blunt afterbody at the base corner. The other tabs were equally spaced circumferentially around the afterbody at 45-deg increments. The spacing between the tabs was such that the circumferentially mounted transducers were either aligned on the centerline of a tab or halfway between two tabs. The second tab configuration examined was a single rectangular strip tab. The strip tab had the following dimensions: a thickness of 0.5 mm ($h/\delta_0 \approx 0.16$), a width of 12.5 mm, and it covered the circumference of the afterbody. This tab was mounted a distance of 12 mm upstream of the base corner, based on results of the previous study.[11] Schematics showing the various tab configurations and the transducer ports on the blunt afterbody are shown in Fig. 2.

Pressure measurements were recorded on the base surface of the blunt afterbody via two methods. The first method used a Pressure Systems, Inc., Netscanner Model 98 RK, which is capable of recording static pressures at a rate of approximately 6 Hz. Measurements obtained in the base region were recorded with Model 9816 modules that have a pressure range of ±0–103 kPa. Because the Netscanner system can only acquire measurements at the limited rate of 6 Hz, it was obviously not capable of recording high-frequency

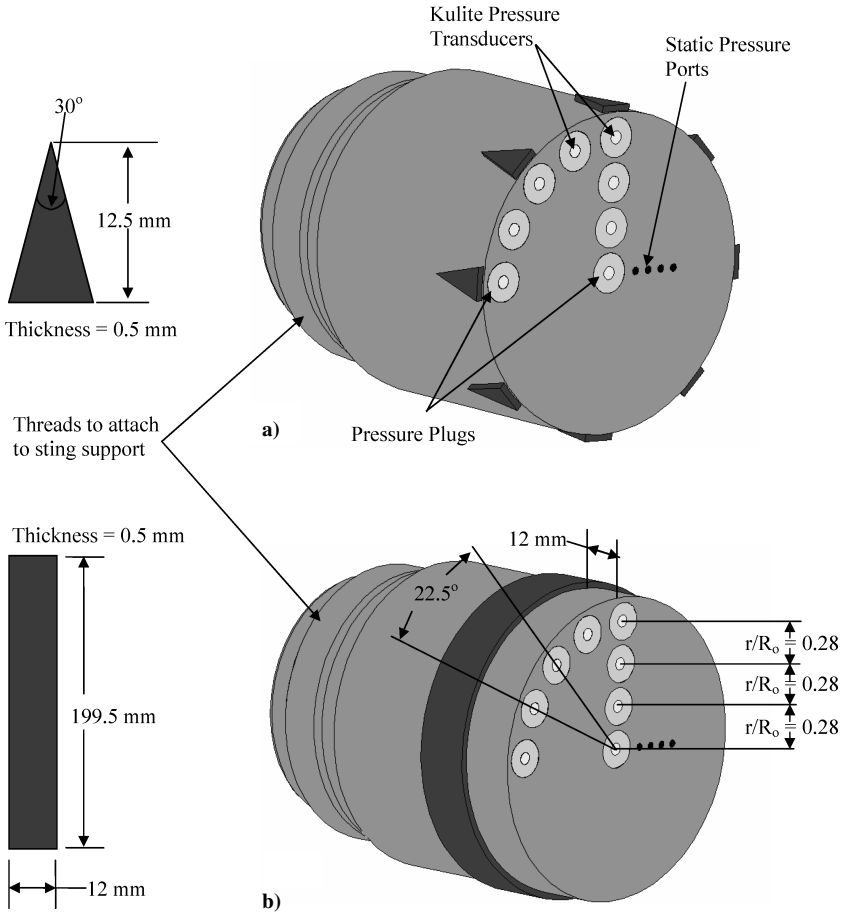

Fig. 2 Blunt afterbody with a) triangle-tab configuration and b) strip-tab configuration.

time-series data. To acquire high-frequency pressure measurements, Kulite pressure transducers, model XCS-062, were used. These transducers have a pressure-sensing capability of 0–68.96 kPa and a maximum frequency range of approximately 60 kHz. As quoted by the manufacturer, these transducers have a measurement uncertainty of 0.25% combined nonlinearity and hysteresis and 0.1% repeatability. The Kulite transducers were mounted flush to the surface and along the centerline axis of threaded plugs. The plugs were inserted into the various radial and circumferential ports along the base of the blunt afterbody, as shown in Fig. 2. The data recorded from the high-frequency pressure transducers were then analyzed using standard time-series analysis methods described by Bendat and Piersol.[14] Data-reduction techniques for these experiments are described in detail by Janssen and Dutton.[13]

Experimental Results

Measurements were obtained and analyzed at four varying radial positions and five varying circumferential positions across the base for both tab-configured afterbodies. Experimental results recorded for the triangle tab-configured afterbody will be discussed first, with the discussion of results recorded for the strip tab-configured afterbody to follow.

Triangle-Tab Configuration

The radial dependence of time-averaged base-pressure measurements normalized by the freestream static pressure is shown in Fig. 3 for the no-tab (blunt) afterbody compared to the triangle-tab configured afterbody. The uncertainty bars in this figure are representative of run-to-run precision uncertainty (one standard deviation) in the recorded data. The time-averaged static-pressure tap measurements, shown as diamonds, and high-frequency pressure measurements, shown as triangles, are in good agreement and display a slight increase in base pressure with increasing radial distance,

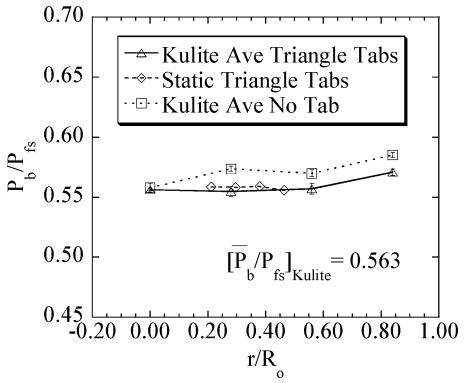

Fig. 3 Time-averaged radial base-pressure measurements for the triangle-tab afterbody and the no-tab afterbody.

as was the case for the no-tab afterbody. The average base pressure is reduced by nearly 2.5% with the addition of the triangular tabs. This reduction in base pressure is not as severe as the 10% reduction in base pressure previously recorded by Bourdon and Dutton on a virtually identical afterbody.[10] Part, if not all, of this difference can be accounted for by the coarse radial resolution of these base-pressure measurements, together with minor differences in the tab geometry and flow conditions between the two sets of experiments. A reduction in base pressure was expected, as previous flowfield visualizations demonstrated that the triangle tabs organize streamwise-oriented vortices in the shear layer that entrain mass from the recirculation region.[10,12] These measurements also demonstrated a less severe change in pressure with increasing radial distance, as compared to the no-tab case. The difference from the highest to the lowest pressure across the base radius with the

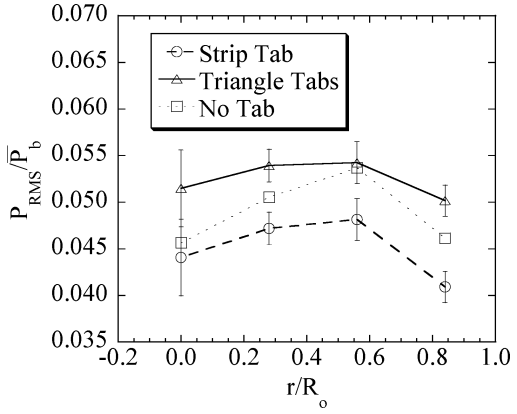

Fig. 4 Radial rms base-pressure measurements for the triangle-tab afterbody and strip-tab afterbody compared to the no-tab afterbody.

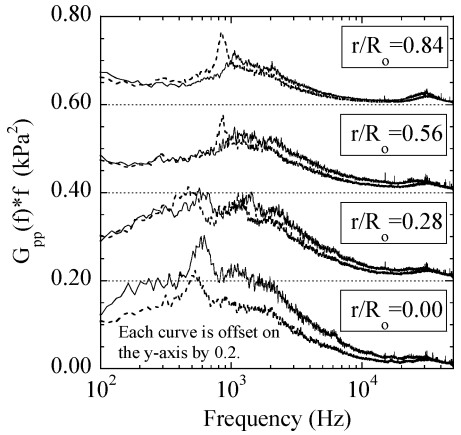

Fig. 5 PSD estimates for varying radial base locations for ——, the triangle tab-configured afterbody and - - - -, the no-tab afterbody.

triangle tabs is approximately 2.8%, around half that measured for the no-tab afterbody.

The circumferential distribution of time-averaged base pressure (not shown) varied by less than 0.33% over the positions investigated (see Fig. 2), demonstrating that the base-pressure distribution is axisymmetric for this tabbed case. This occurs even at the outermost radial position measured, despite the fact that the tabs introduce discrete streamwise-oriented vortices around the circumference of the shear layer.

Figure 4 presents the radial rms distribution of the base-pressure fluctuations normalized by the mean base pressure for both the triangle-tab afterbody and the strip-tab afterbody compared to the no-tab case. The dimensionless rms values are higher for the triangle-tab afterbody than those for the no-tab afterbody and are approximately 5.3% of the mean base pressure on average. Similar to the time-averaged base-pressure measurements, the dimensionless rms values show a very slight increase with increasing radial position, until the outermost location where the rms level drops. The increased rms levels suggest that the physical mechanism responsible for increased shear-layer mixing, the streamwise vortices in the shear layer generated by the triangle tabs, is at least partially responsible for the increased base-pressure fluctuations. Circumferentially measured rms values varied by about 2.6% from position to position. As before for the time-averaged circumferential pressure measurements, no trend was revealed based on the position of the triangular tabs relative to the position of the pressure transducers. As a result, it can be concluded that the effect of additional streamwise vorticity caused by the tabs is relatively localized within the shear layer and is not measurable via high-speed transducers on the base at the outermost radial location considered in this investigation.

Power-spectral-density (PSD) estimates for the triangular-tab configuration compared to the no-tab configuration at varying radial locations are shown in Fig. 5. As for the no-tab afterbody, the PSD estimates for the triangle-tab configuration demonstrate a distinct change in the energy distribution with radial position. At the two innermost locations, $r/R_0 = 0.0$ and 0.28, the fluctuating pressure energy is higher at nearly all frequencies below 1 kHz for the triangular-tab case than for the no-tab afterbody. The center location, $r/R_0 = 0.0$, displays a well-defined peak at about 600 Hz, which is slightly higher than the 500-Hz peak observed at this location for the no-tab afterbody. The second innermost location, $r/R_0 = 0.28$, displays two smaller peaks, one corresponding to the 600-Hz peak at the center location and the other at approximately 1450 Hz. Although the PSDs for the two innermost locations are qualitatively similar to those for the no-tab afterbody, those for the two outermost locations show a significant difference. The two outermost location PSDs lack the distinct peaks seen at 850 Hz for the no-tab afterbody. Rather, the PSDs at these locations for the triangular tabs show a gradual increase to approximately 1000 Hz, where slight peaks occur. Perhaps the lack of distinct peaks in the PSDs at these locations could be caused by the distortion of circumferential vorticity caused by the discrete placement of the tabs around the afterbody periphery. Upon reaching these slight peaks at 1000 Hz, the PSDs at the two outer radial locations begin to decline at approximately the same rate as for the no-tab afterbody. The PSD at the outermost location, $r/R_0 = 0.84$, also demonstrates a more significant peak centered near 30 kHz, in comparison with the no-tab case. This peak could be associated with turbulent structures in the free shear layer that have been altered by the tabs to more vigorously interact with the recirculation region, causing larger base-pressure fluctuations at the corresponding frequency. Finally, the PSD estimates for the triangle tabs at all radial locations display more energy at frequencies above 1000 Hz than for the no-tab case. This reveals that increased mixing in the shear layer, caused by the streamwise vorticity introduced by the tabs, increases the pressure fluctuations, particularly at these higher frequencies.

Because the triangle-tab configuration disrupts the purely axisymmetric geometry of the no-tab afterbody, it is possible that the base-pressure fluctuations could vary circumferentially for the tabbed case. The outermost radial locations should be particularly sensitive to this change as they are nearest to the tab-altered shear layer. To investigate this, time-series pressure measurements were recorded at $r/R_0 = 0.84$ at the circumferential positions $\theta = 0$, 45, and 90 deg with pressure transducers aligned on the tab centerline and at the circumferential positions $\theta = 22.5$ and 67.5 deg with pressure transducers aligned on the centerline between two tabs, as shown in Fig. 2. The PSD estimates at these circumferential locations are presented in Fig. 6. As can be seen in this figure, the position of the tabs relative to the transducer has essentially no effect on the corresponding PSD estimate because all locations demonstrate nearly identical PSDs. Thus, it is concluded that the changes in shear-layer entrainment and mixing caused by the triangle-tab configuration affect base-pressure fluctuations in a global, not local, manner, at least at the radial location of $r/R_0 = 0.84$. Measurements closer to the base edge, however, can show nonaxisymmetric effects of the discrete tab placement.

The base-pressure fluctuations for the triangle-tab geometry are further quantified in Figs. 7 and 8 by the skewness and kurtosis values obtained from the probability density function (PDFs) of the time-series measurements. Skewness and kurtosis values are defined by the respective equations:

$$\text{Skew} = \frac{1}{N_t}\sum_{i=1}^{N_t}\left(\frac{x_i - \bar{x}}{\hat{x}}\right)^3 \tag{1}$$

$$\text{Kurt} = \frac{1}{N_t}\sum_{i=1}^{N_t}\left(\frac{x_i - \bar{x}}{\hat{x}}\right)^4 \tag{2}$$

The skewness values (Fig. 7) are significantly higher for the triangle-tab configuration than for the no-tab configuration, indicating the occurrence of more and/or larger high-pressure fluctuations. This indicates that the increase in base-pressure fluctuations for the triangle tabs might be the result of high-pressure fluid from the shear layer being turned back intermittently toward the base in the reattachment

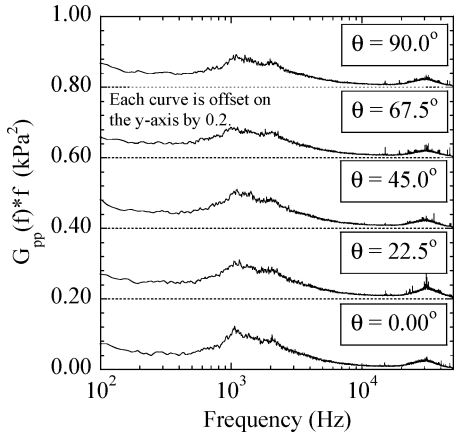

Fig. 6 PSD estimates for varying circumferential locations along the triangle-tab-configured afterbody.

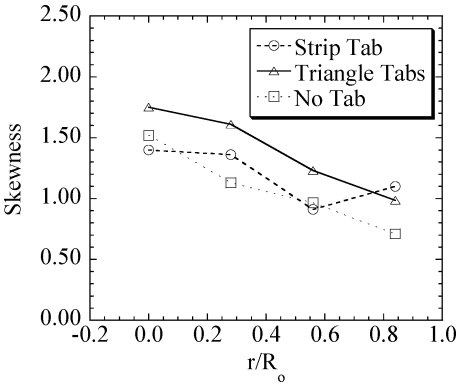

Fig. 7 Skewness values of the time-series pressure measurements for the triangle-tab, strip-tab, and no-tab configurations.

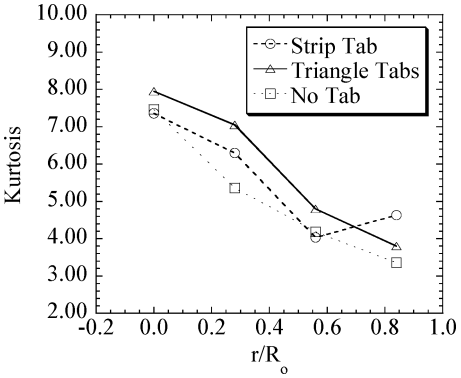

Fig. 8 Kurtosis values of the time-series pressure measurements for the triangle-tab, strip-tab, and no-tab configurations.

region. Similar to the no-tab case,[13] the skewness values also decrease with increasing radial distance. Kurtosis values (Gaussian value $= 3.0$) are also higher at all radial positions for the triangle-tab afterbody in comparison to the no-tab afterbody, Fig. 8. These results emphasize that pressure fluctuations are larger in magnitude and occur increasingly more toward the high-pressure side as compared to the no-tab case. Thus, the increase in high-pressure fluctuations is most likely not a result of increased shear-layer flapping or recirculation-region motions, but more likely is caused by energized turbulent structures that are returned toward the base at reattachment. Indeed, flowfield visualizations by Bourdon and Dutton[10] demonstrated that turbulent structures in the triangle tab-altered shear layer are larger and better organized than for the no-tab case.

Results from simultaneous dual-transducer measurements at varying combinations of radial positions are presented in Figs. 9

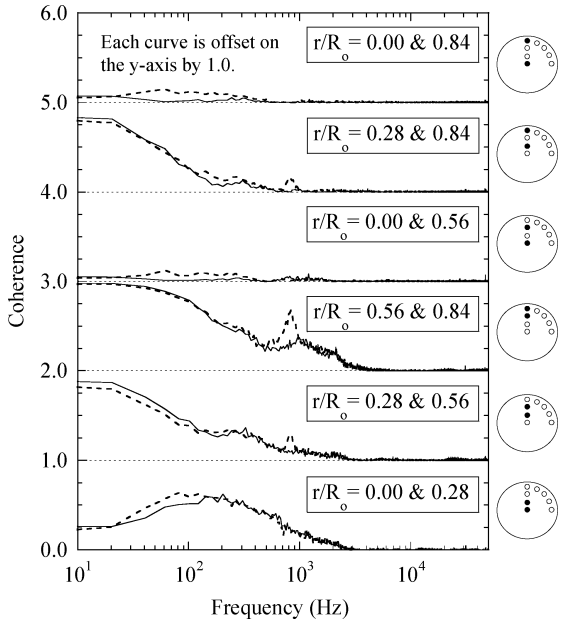

Fig. 9 Coherence coefficient at varying combinations of radial positions for ——, the triangle tab-configured afterbody and - - - -, the no-tab afterbody.

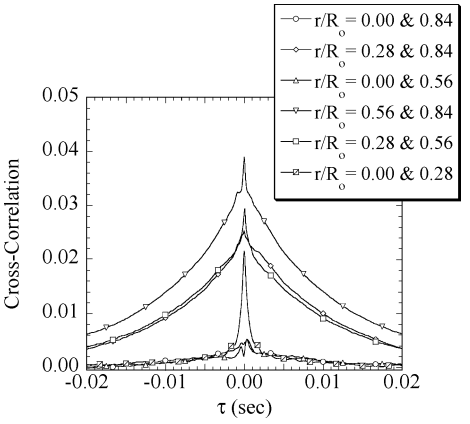

Fig. 10 Cross-correlation coefficient at varying combinations of radial positions for the triangle tab-configured afterbody.

and 10. The coherence function measures the extent to which simultaneously-sampled measurements are linearly related to each other. Estimation of the coherence function is achieved by

$$\gamma_{xy}^2 = \frac{|G_{xy}(f_k)|^2}{G_{xx}(f_k)G_{yy}(f_k)} \tag{3}$$

where $G_{xy}(f_k)$ is the one-sided cross-spectral density function and $G_{xx}(f_k)$ and $G_{yy}(f_k)$ are the PSD estimates of time-series records for $x(t)$ and $y(t)$, respectively. Coherence results, shown in Fig. 9, are similar to those for the no-tab afterbody. The center location shows nearly zero coherence with the two outermost radial locations at all frequencies. Modest coherence levels in the frequency range of 100–1000 Hz are observed for the center location in combination with the second innermost location ($r/R_0 = 0.0$ and 0.28). The second innermost location ($r/R_0 = 0.28$) also displays modest levels of coherence with the two outermost locations ($r/R_0 = 0.56$ and 0.84) at frequencies less than 100 Hz. Relatively high levels of coherence are demonstrated between the two outermost locations ($r/R_0 = 0.56$ and 0.84) at frequencies less than 1 kHz. The most noticeable difference between the triangle-tab configuration and the no-tab configuration occurs for the coherence between the two outermost locations. The distinct peak, which occurs near 850 Hz for the no-tab afterbody, is noticeably absent in the triangle-tab PSD estimate, resulting in a significant reduction in coherence near this

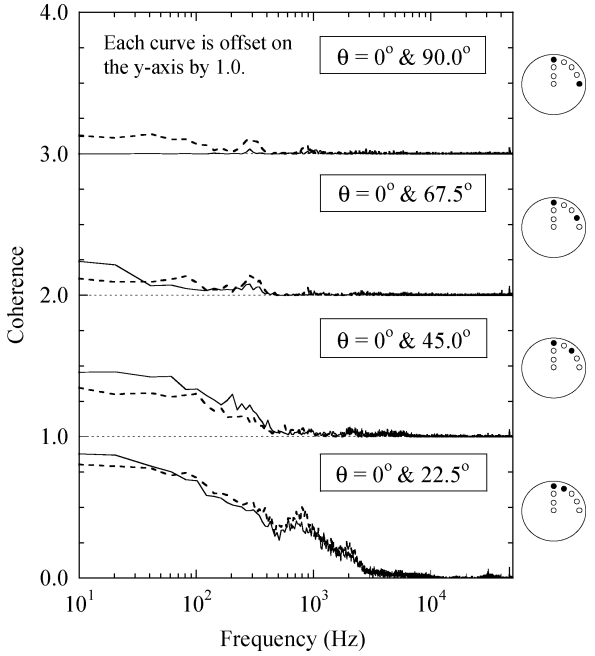

Fig. 11 Coherence coefficient at varying combinations of circumferential positions for ——, the triangle tab-configured afterbody and - - - -, the no-tab afterbody.

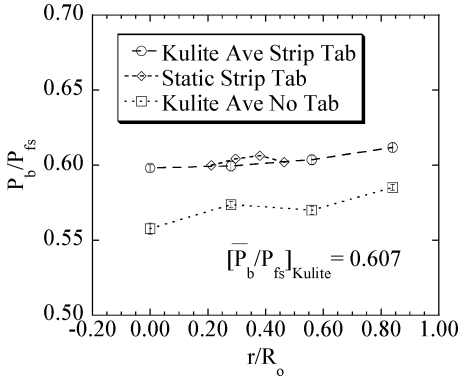

Fig. 12 Time-averaged radial base-pressure measurements for the strip-tab afterbody and the no-tab afterbody.

frequency. Taken as a whole, these results demonstrate that although the frequency content of the pressure fluctuations (i.e., PSDs) has changed somewhat because of the addition of the triangle tabs, the coherence characteristics of the dual-transducer time series measured along the base are relatively unaltered.

Cross-correlation coefficient results, shown in Fig. 10, further exhibit the independence of the pressure histories experienced by the center and the two outermost locations, because the results are nearly zero for all time delays. All other combinations of radial positions show distinct peaks centered at zero time delay, indicating that the dominant mechanism responsible for base-pressure fluctuations affects all of these radial positions essentially simultaneously. However, these cross-correlation plots lack the well-defined secondary peaks that were previously observed for the no-tab case.[13] These secondary peaks were thought to correlate with pressure disturbances convecting with the local flow along the base. Perhaps these pressure disturbances are much weaker for the triangle-tab case or other pressure fluctuation mechanisms that are enhanced by the triangle tabs obscure the correlations of these (local) pressure fluctuations.

Dual-transducer measurements were also obtained at varying combinations of circumferential positions at the outer radial location $r/R_0 = 0.84$. These measurements can be observed in the circumferential coherence plot (Fig. 11). Coherence results for adjacent pressure transducers (22.5-deg spacing) are relatively high up to a frequency of 1000 Hz. As the circumferential spacing is increased, the coherence drops significantly. At the largest circumferential spacings (67.5 and 90 deg), the coherence is essentially zero at all frequencies. The results from these experiments are nearly identical to those for the no-tab case.[13] Because the transducers display nearly identical levels of circumferential coherence with the no-tab afterbody, even though Bourdon and Dutton previously recorded images revealing the organization of streamwise vortices in the shear layer for the tabbed case,[10] the effects on base pressure are realized globally, not locally.

Strip-Tab Configuration

The strip-tab configuration, as previously demonstrated through time-averaged base-pressure measurements and flowfield visualizations by Bourdon and Dutton,[11] decreases mixing in the free shear layer, decreases mass entrainment from the recirculation region, and, thereby, increases base pressure. Figure 12 demonstrates the effect on time-averaged base pressure when adding the strip tab. As seen in this figure, the time-averaged base pressure is increased by approximately 5% over that for the no-tab afterbody. Previous static-pressure tap measurements recorded by Bourdon and Dutton[11] demonstrated a base pressure increase of approximately 3% over the no-tab afterbody. This discrepancy can again be accounted for by the relatively coarse radial spatial resolution of the current measurements together with minor differences between the flow conditions and tab geometry for the two sets of experiments.

The increase in time-averaged base pressure is accompanied by a decrease in the normalized rms pressure-fluctuation levels, as shown in Fig. 4. Normalized rms levels for the strip-tab configuration are the lowest of the experimental geometries investigated at approximately 4.4% of the mean base pressure on average. As observed with all other geometries studied, the rms levels increase with increasing radial distance, until the outermost location where the rms value drops. For cases for which the rms levels decrease (e.g., strip tab), the area-averaged base pressure $\overline{P}_b$ increases. Thus, the effect on the dimensional pressure fluctuation magnitude is less severe than Fig. 4 suggests because of normalization with $\overline{P}_b$. Imaging work completed by Bourdon and Dutton[11] revealed that side-view shear-layer flapping, normalized by the average shear-layer thickness, is increased at all measurement locations with the addition of a strip tab. The reduced base-pressure rms levels for this case then seem to suggest that shear-layer flapping is not a primary mechanism contributing to base-pressure fluctuations. Other near-wake motions, such as end-view centroidal motion and recirculation region area pulsing, are slightly higher near separation with the strip tab but tend to be much lower at downstream locations in the near-wake region.[12] A reduction in these motions, therefore, can play a role in the reduced rms levels measured for the strip-tab configuration. As a result, the strip tab seems to stabilize some motions of the shear layer and recirculation region, thereby reducing pressure fluctuation magnitudes.

PSD estimates at varying radial positions for the strip-tab case are shown in Fig. 13 and compared with previous measurements for the no-tab afterbody. The PSDs are similar qualitatively to those for the no-tab case, shown by the dashed lines, except at reduced magnitudes, corresponding to the lower rms levels previously observed and discussed for the strip tab. The innermost location for the strip tab demonstrates a peak at approximately 480 Hz, compared to 500 Hz for the no-tab afterbody. Most notably, the distinct peaks at the two outermost locations that were absent for the triangle-tab configuration do appear for the strip-tab configuration. The distinct peak in this case is found to occur near 820 Hz ($St = 0.091$), as opposed to 850 Hz, as was seen in the no-tab case. A noticeable trend for the frequency at which the distinct peaks occur is observed based on the time-averaged base pressure. As the mean base pressure is increased, the frequency at which the peak occurs is found to decrease. This finding also holds true for the triangular-tab configuration if the slight peak occurring at 1000 Hz is selected as its distinct peak. As a result, it can be inferred that as the recirculation region becomes longer, because of increased base pressure, the distinct peaks at the

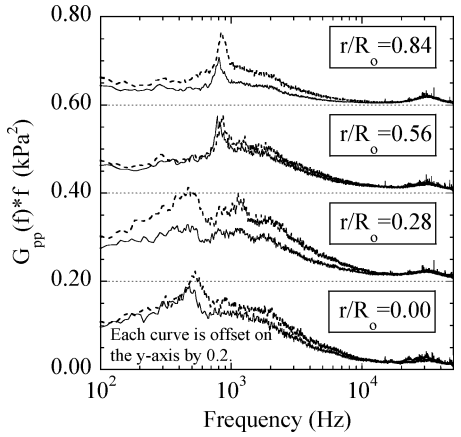

Fig. 13 PSD estimates for varying radial base locations along ——, the strip tab-configured afterbody and - - - -, the no-tab afterbody.

outermost radial locations shift to lower frequencies. This can indicate that some sort of longitudinal acoustic interaction is responsible for these particular peaks in the PSD estimates. Finally, a smaller peak, centered near 30 kHz, is again observed at the two outermost locations. A significant reduction in high-frequency energy content, above 1 kHz, for the strip tab is realized at all radial locations in comparison with the triangular-tab and no-tab configurations. Bourdon and Dutton[11] noted that the average turbulent structure size is not significantly altered in the side view for the strip tab, but is slightly smaller in the end view. Thus, it seems that the damping of turbulent structures by the strip tab results in a reduction in high-frequency pressure oscillations in the base region.

Decreased kurtosis values confirm that the PDFs of the pressure histories obtained along the base for the strip tab are more Gaussian and less peak shaped at all locations, except for the outermost location, than for the triangle-tab case, as shown in Fig. 8. Similar to all other geometries investigated, the skewness values displayed in Fig. 7 are positive because of the dominant high-side pressure fluctuations. The skewness and kurtosis results for the strip-tab configuration demonstrate a unique result at the outermost location, $r/R_0 = 0.84$. Measurements on the other afterbodies show that with increasing radial distance, the skewness and kurtosis values decline monotonically. However, at the outermost location for the strip-tab case the kurtosis and skewness values increase over those recorded for the second outermost location, $r/R_0 = 0.56$. The reason for this increase is unknown, but might be related to some sort of vortex shedding or instability amplification mechanism that is enhanced by the strip tab, leading to more high-pressure fluctuations and a more peaked PDF at the outermost radial location.

Coherence and cross-correlation results for varying combinations of radial positions are plotted in Figs. 14 and 15, respectively, for the strip-tab configuration. These results are similar in most respects to those for the no-tab geometry. The coherence results show that the two outermost locations are nearly statistically independent of the center location. The second innermost location shows modest levels of coherence with the two outermost locations at low frequencies and with the center location at midrange frequencies. Additionally, the two outermost locations demonstrate high to modest levels of coherency for frequencies less than 1000 Hz, especially in the vicinity of the 820-Hz peak displayed in the PSDs, as shown in Fig. 13. A small difference between the strip-tab and no-tab results is that the coherence values are modestly higher for the strip tab for frequencies below 100 Hz.

The cross-correlation coefficient results in Fig. 15 demonstrate relatively strong peaks at zero time delay for all combinations of radial positions, with the exception of the center location in combination with the two outermost locations. Small secondary peaks are observed between the combinations $r/R_0 = 0.28$ and 0.56, $r/R_0 = 0.28$ and 0.84, and $r/R_0 = 0.56$ and 0.84. Such secondary peaks were found to correlate with pressure disturbances convecting with the recirculating flow along the base from previous laser-

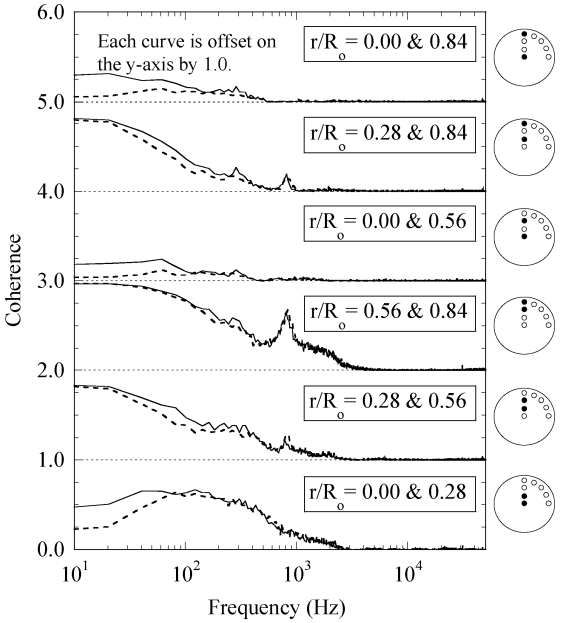

Fig. 14 Coherence coefficient at varying combinations off radial positions for ——, the strip tab-configured afterbody and - - - -, the no-tab afterbody.

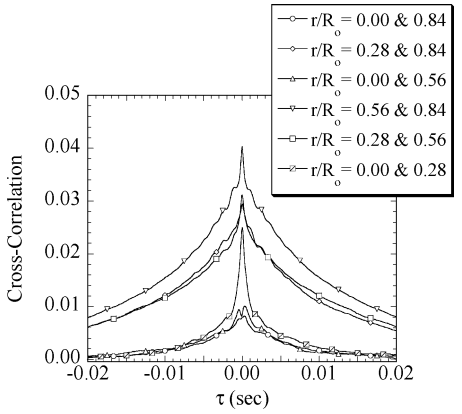

Fig. 15 Cross-correlation coefficient at varying combinations of radial positions for the strip tab-configured afterbody.

Doppler-velocimetry measurements for the no-tab case.[1,13] It is assumed that a similar conclusion can be drawn in this case, although no velocity measurements for these tabbed geometries exist. The low levels of cross correlation between the center location and the two outermost locations lends further credence to the conclusion that distinct pressure histories are experienced by these locations.

Conclusions

Single- and dual-transducer high-frequency pressure measurements were recorded at varying radial and circumferential locations along the base of a blunt cylindrical afterbody modified with two different sub-boundary-layer disturbances. Measurements were recorded at a freestream Mach number of 2.46. The high-frequency pressure measurements were analyzed using standard time-series analysis techniques to examine the dynamic effects of the sub-boundary-layer disturbances on base pressure. The conclusions from these experiments are discussed next.

1) The time-averaged base-pressure distribution was altered by the two tab configurations in opposite directions. The triangle-tab configuration decreased the mean base pressure by approximately 2.5%, whereas the strip-tab configuration increased base pressure by approximately 5.0% over the no-tab afterbody. Both tab configurations decreased the radial variation in base pressure slightly compared to the no-tab case.

2) Normalized rms magnitudes were observed to increase or decrease corresponding to the decrease or increase, respectively, of the mean base pressure. This can partially be attributed to the increase or decrease in the recirculation region size with base pressure, suggesting some sort of acoustical effect. RMS measurements were compared with flowfield visualizations of the strip-tab configuration that quantified shear-layer flapping and were found not to correlate with these motions. However, other motions of the recirculation region, such as end-view centroidal motion and recirculation region pulsing, were found to decrease as pressure fluctuation magnitudes decrease.

3) The power-spectral-density (PSD) estimates are considerably different for the two tab-configured afterbodies. The triangle-tab PSDs lack the distinct peak typically observed in the 800–900-Hz range for the no-tab afterbody and the strip-tab afterbody. These results imply that the triangle tabs alter the shear layer in some manner so as to suppress pressure fluctuations from the (unknown) mechanism that causes fluctuations in that frequency range. Perhaps the discretely placed tabs and their associated streamwise vorticity alter the circumferential vorticity distribution, thereby reducing this particular peak.

4) The triangle-tab configuration demonstrated increased pressure fluctuations at frequencies above 1000 Hz compared to the strip-tab and no-tab cases. A peak in the PSD estimate near 30 kHz is also larger for the triangle-tab afterbody than for the no-tab and strip-tab afterbodies. These results suggest that turbulent structures in the shear layer are energized more by the triangle tabs and, thus, interact more vigorously with the recirculation region. As a result of these interactions, more mass is entrained into the shear layer, and the average base pressure is decreased.

5) Circumferential pressure histories on the triangle tab-configured afterbody investigated potential local effects of the sub-boundary-layer disturbances. No differences were observed from measurements recorded at various circumferential positions for the outermost radial location. Thus, the effects on base pressure caused by the sub-boundary-layer disturbance tabs are axisymmetric and global, at least at the outermost location measured in this study.

6) Dual-transducer measurements were qualitatively similar to measurements recorded for the no-tab afterbody. The coherence measurements imply quite distinct pressure histories at the center and two outermost locations, while moderately high correlation exists between the two outermost locations. Cross correlations suggest that a zero time delay is dominant for nearly all measurement locations with modest levels of coherence. This suggests that a mechanism that affects base-pressure fluctuations does so in a global manner.

Acknowledgments

This work was sponsored by the U.S. Army Research Office under Grant DAAD19-01-1-0367 and was monitored by Thomas L. Doligalski. This support is gratefully appreciated.

References

[1]Herrin, J. L., and Dutton, J. C., "Supersonic Base Flow Experiments in the Near Wake of a Cylindrical Afterbody," *AIAA Journal*, Vol. 32, No. 1, 1994, pp. 77–83.

[2]Smith, K. M., and Dutton, J. C., "Investigation of Large-Scale Structures in Supersonic Planar Base Flow," *AIAA Journal*, Vol. 34, No. 6, 1996, pp. 1146–1152.

[3]Rollstin, L., "Measurement of Inflight Base-Pressure on an Artillery-Fired Projectile," AIAA Paper 87-2427, Aug. 1987.

[4]Dolling, D. S., Fournier, E., and Shau, Y. R., "Effects of Vortex Generators on the Growth of a Compressible Shear Layer," *Journal of Propulsion and Power*, Vol. 8, No. 5, 1992, pp. 1049–1056.

[5]Samimy, M., Zaman, K. B. M. Q., and Reeder, M. F., "Effect of Tabs on the Flow and Noise Field of an Axisymmetric Jet," *AIAA Journal*, Vol. 31, No. 4, 1993, pp. 609–619.

[6]Papamoschou, D., "Structure of the Compressible Turbulent Shear Layer," AIAA Paper 89-0126, Jan. 1989.

[7]King, C. J., Krothapalli, A., and Strykowski, P. J., "Streamwise Vorticity Generation in Supersonic Jets with Minimal Thrust Loss," AIAA Paper 94-0661, Jan. 1994.

[8]Krothapalli, A., Strykowski, P. J., and King, C. J., "Origin of Streamwise Vortices in Supersonic Jets," *AIAA Journal*, Vol. 36, No. 5, 1998, pp. 869–872.

[9]Island, T. C., Urban, W. D., and Mungal, M. G., "Mixing Enhancement in Compressible Shear Layers via Sub-Boundary Layer Disturbances," *Physics of Fluids*, Vol. 10, No. 4, 1998, pp. 1008–1020.

[10]Bourdon, C. J., and Dutton, J. C., "Mixing Enhancement in Compressible Base Flows via Generation of Streamwise Vorticity," *AIAA Journal*, Vol. 39, No. 8, 2001, pp. 1633–1635.

[11]Bourdon, C. J., and Dutton, J. C., "Altering Turbulence in Compressible Base Flow Using Axisymmetric Sub-Boundary-Layer Disturbances," *AIAA Journal*, Vol. 40, No. 11, 2002, pp. 2217–2224.

[12]Bourdon, C. J., "Flow Visualizations and Measurements of Turbulent Structures in Drag-Altered Axisymmetric Compressible Base Flows," Ph.D. Dissertation, Dept. of Mechanical and Industrial Engineering, Univ. of Illinois, Urbana, IL, June 2001.

[13]Janssen, J. R., and Dutton, J. C., "Time-Series Analysis of Supersonic Base-Pressure Fluctuations," *AIAA Journal*, Vol. 42, No. 3, 2004, pp. 605–613.

[14]Bendat, J. S., and Piersol, A. G., *Random Data Analysis and Measurement Procedures*, Wiley, New York, 2000.

P. Weinacht
Associate Editor